Competition between Chain Extension and Crosslinking in Polyamide 1012 during High Temperature Thermal Treatments as Revealed by SSA Fractionation

Xuan Li,[1,2] *Lili Wang,*[1,3] *Dujin Wang,*[1,2] *Alejandro J. Müller,*[4,5,]* *and Xia Dong*[1,2,]*

[1]Beijing National Laboratory for Molecular Science, CAS Key Laboratory of Engineering Plastics, Institute of Chemistry, Chinese Academy of Sciences, Beijing 100190, P. R. China

[2]University of Chinese Academy of Sciences, Beijing 100049, P. R. China

[3]State Key Laboratory of Biofibers and Eco-textiles, Collaborative Innovation Center for Marine Biomass Fibers, Materials and Textiles of Shandong Province, Institute of Marine Biobased Materials, Qingdao University, Qingdao 266071, P. R. China

[4]POLYMAT and Department of Polymers and Advanced Materials: Physics, Chemistry and Technology, Faculty of Chemistry, University of the Basque Country UPV/EHU, Donostia-San Sebastián 20018, Spain

[5]Ikerbasque, Basque Foundation for Science, Bilbao, Spain

*Corresponding authors: alejandrojesus.muller@ehu.es and xiadong@iccas.ac.cn

ABSTRACT: Self-nucleation and annealing (SSA) is an efficient way to thermally fractionate semi-crystalline polymers. The thermal fractions produced by SSA have distinct melting points that correspond to different average lamellar thickness. In this research, SSA was adopted to investigate the in-situ evolution of lamellar thickness of polyamide 1012 (PA1012), which was affected by high temperature thermal treatments. SSA successfully fractionated PA1012 into 4 thermal fractions with different average lamellar thicknesses. The integrated area of the first or second SSA fraction against the total endothermic integrated area was plotted as a function of thermal treatment time to study the kinetics of lamellar thickness changes. Two opposing structural effects, chain growth and crosslinking, occurred during the applied thermal treatment (which consisted in thermally treating the material by holding it isothermally at temperatures in the range of 140-250 ºC) and they were detected as a function of time by SSA, rheology and dissolution behavior. The structural changes increased the viscosity and T_g and decreased the overall crystallization rate. Based on the construction of a master curve of "time-temperature superposition" at a reference temperature (T_0) of 190 ºC, the mechanism for lamellar thickness evolution was divided into three stages: (a) Stage I: Initially, PA1012 end groups reacted rapidly with active sites to generate chemically crosslinked structures. (b) Stage II: As the number of end groups rapidly increased, amidation reactions between carboxylic end groups and amine end groups resulted in linear chain growth. Linear chain growth and crosslinking occurred simultaneously, and there was no change in lamellar thickness or its distribution. (c) Stage III: Eventually,

an increasing number of end groups was formed in the system, most of which led to linear chain growth via chain end-group reactions. These structural changes during the applied thermal treatments enhanced the mechanical properties and the heat resistance of PA1012. This work provides specific guidance for improving the toughness, strength and heat resistance of polyamide materials.

KEYWORDS: Long chain polyamides; Lamellar thickness; Chemical crosslinking; Linear chain growth; Successive self-nucleation and annealing (SSA)

INTRODUCTION

Long chain polyamides (LCPAs) are polyamides in which the number of methylene groups between adjacent amide groups on the main chain is no less than 10. Compared with traditional commercial polyamides, for example PA6 or PA66, LCPAs have a lower proportion of amide groups per repeating unit, which imparts lower water absorption, higher elongation at break, better balance of rigidity and toughness, more desirable dimensional stability and better performance in molding.

LCPAs can be synthesized via condensation polymerization between dicarboxylic acids and diamines, where dicarboxylic acids are converted into diamines. Dicarboxylic acids can currently be obtained either by chemical synthetic methods, which are dangerous and can produce hazardous byproducts, or by biological fermentation methods. The latter method uses the unique oxidizing ability of microorganisms and

the catalysis of enzymes in cells to ferment the byproducts of petroleum containing various n-alkanes (carbon chain length is 9-16); this occurs at room temperature and pressure and then methyl groups at both ends of n-alkanes are oxidized into carboxyl groups to form various long-carbon chain dibasic acids with corresponding chain lengths. Biological fermentation methods have attracted particular interest in recent years due to their environmentally friendly conversion processes with biobased materials and mild conditions. Therefore, some LCPAs, such as PA1010, PA1012, and PA1212, have been developed rapidly by using monomer preparation technology based on bio-fermented sources.

The development of LCPAs mainly focuses on high-performance and multi-functional modification[1-4]. Recently, there have been some studies on the structure of condensed states of LCPAs[5-7], and especially on the structure-property relationship of LCPAs subjected to different external fields. Zhou et al.[8] studied the relationship between amide group density and dielectric properties of PA11, PA12, PA1012 and PA1212. Yang et al.[9] investigated the melting and crystallization behavior of PA1010 under different pressure fields, and they found that lower pressures and higher pressures led to different crystal forms and that a crosslinked structure was generated without crystallization under medium pressures. Gao et al.[10] dealt with the effects of a complex flow field on the crystallization and orientation behavior of PA1012, which involved the coupling of extensional and shear flow in a narrow channel. These finally resulted in a special five-layer structure formed during this process.

Tashiro et al.[11-12] used Fourier-transform infrared spectroscopy (FTIR), X-ray diffraction (XRD) and molecular dynamics calculations to investigate the structural changes of PA1010 that occurred during heating to temperatures near the Brill transition temperature. They found that the bands of the methylene segments, corresponding to the all-trans segmental parts (-$(CH_2)_n$- (n=10, 8)), decreased in intensity and finally disappeared in the Brill transition, while some new bands corresponding to the all-trans segmental parts (-$(CH_2)_n$- (n=7, 5)), appeared. This indicated that the lengths of the all-trans segmental parts became shorter because the methylene segments became conformationally disordered due to interruptions by some gauche segmental parts. Wang et al.[13] studied the polymorphism transition, lamellar evolution and lamellar orientation of PA1012 induced by deformation at three temperatures, 30 ºC (below T_g), 60 ºC (close to T_g) and 100 ºC (above T_g); this involved the use of the Synchrotron Radiation Facility and correlations between tensile properties and microstructures were identified. The results showed that stretching-induced crystallization occurred during stretching at temperatures above the glass transition temperature (T_g), which led to higher breaking strength and elongation.

Because of the nature of condensation polymerization, the residual end groups of LCPAs are still reactive. This leads to complex structural evolution of LCPAs with multiple factors operating at temperatures above T_g. Solid-state polymerization (SSP)[14-15] occurred via reactions of the chain end groups of LCPAs at temperatures between T_g and the onset temperature of melting ($T_{m,onset}$), resulting in a second increase in

molecular weight. Some researchers have studied the effects of SSP factors, including polymerization pressure[16] and the initial viscosity[17-18], on the kinetics of molecular weight changes (represented by intrinsic viscosity) in LCPAs.

When the materials are prepared or processed, they remain at relatively high temperatures for a period of time. However, there are few studies on the structural evolution of LCPAs at higher temperatures, especially at those above $T_{m,onset}$. Liu et al. studied the evolution of the rheological properties of PA1012 during isothermal processes occurring in the molten state[19].

In the present work, we have studied the structural evolution of PA1012 chains, and their self-assembly into crystals, occurring during post-polymerization reactions caused by selected thermal treatments. The successive self-nucleation and annealing (SSA) method was used to fractionate PA1012 by differential scanning calorimetry (DSC), which exhibited better fractionation efficiency and resolution than other previously used methods and did not involve any solvents[20]. SSA is a well-established thermal fractionation technique that was designed and implemented by Müller et al. in 1997[21]. It exploits the molecular segregation capacity of semi-crystalline polymer systems by involving both intra- and intermolecular fractionation. DSC[22] was used to study self-nucleation and the effects of hydrogen bond stability on the memory effects in the crystallization of LCPAs.

In this study, we first used SSA to investigate the evolution of lamellar thickness of PA1012 in situ; this evolution was affected by various thermal processes. We found

that there were two structural changes, linear chain growth and chemical crosslinking, that occurred during the thermal treatment, and these were distinguished by SSA according to their contrasting contributions to lamellar thickness. The integrated area of the first or second fraction against the total integrated area as a function of treatment time was plotted to determine the kinetics of the lamellar thickness and its distribution evolution. There was a "time-temperature equivalence" phenomenon observed by shifting and superposing the curves for different temperatures to build the main curve at a reference temperature (T_0) of 190 ºC. The mechanism for evolution of the lamellar thickness of PA1012 was determined for the first time. We also studied the effects of structural changes on the performance of the material upon thermal treatment and this work could provide guidance for studies of thermal structural evolution of all AABB type PAs and subsequent design of high-performance materials.

EXPERIMENTAL SECTION

Materials

The PA1012 resins used in this research were provided by Shandong Guangyin New Material Co., Ltd., and exhibited a melting temperature T_m=188°C. The melt flow index of this material was 1.0 g/10 min, as determined at 235 °C according to ASTM D1238 (2.16 kg). The pellets of PA1012 were dried in a vacuum oven at 80 °C for 24 h before experiments.

Differential Scanning Calorimetry (DSC)

TA Q2000 DSC and PerkinElmer 8500 DSC instruments were both employed for the following studies. The instruments were calibrated before measurements according to the experimental conditions to be used. All experiments were performed under high purity nitrogen. Sample weights of 5 mg were used. Isothermal crystallization experiments and T_g measurements needed rather fast cooling rates, which could be realized by a PerkinElmer 8500 DSC. The PerkinElmer 8500 DSC was equipped with a controlled LN_2 accessory using a liquid nitrogen cooling system (LNCS). Other DSC experiments were performed in a TA Q2000 DSC.

Thermal Fractionation by Successive Self-nucleation and Annealing (SSA)[20, 23]. SSA should be designed by employing the ideal self-nucleation temperature[23] ($T_{s,ideal}$) as the first $T_{s,1}$. Before the SSA procedure, self-nucleation (SN) was performed to find $T_{s,ideal}$, which is described in Figure S1 and S2. According to the results, the $T_{s,ideal}$ was 191 ºC. We applied the same SSA procedures to all samples. The SSA procedures are described in Figure 1a:

(a) The sample was melted for 3 min at 220 °C to erase the thermal history and crystalline memory.

(b) Then, it was cooled at 20 °C/min down to 100 °C to create a standard semi-crystalline state and it was held for 3 min at 100 ºC for thermal equilibration.

(c) The sample was heated from 100 ºC at 20 °C/min up to a chosen T_s and held there for 5 min. Therefore, 5 minutes was the selected fractionation time.

(d) Then, it was again cooled at 20 °C/min down to 100 ºC so that the fraction of the

sample that was melted at T_s crystallized during cooling.

(e) Steps (c) and (d) were repeated at progressively lower T_s values. The interval between T_s temperatures, or fractionation window, was set as 5 °C. The total number of T_s temperatures (including $T_{s,1} = T_{s,ideal}$) was 5.

(f) Finally, the sample was heated at 20 °C/min up to 220 °C.

The final heating DSC scan revealed the SSA fractionation profile of the sample. Since no annealing occurred at $T_{s,ideal}$, the number of produced fractions was equal to four. These four fractions have different average melting points and their four melting peaks can be considered to have four different average lamellar thicknesses, as proven earlier in different materials by SAXS (see references[23-24]).

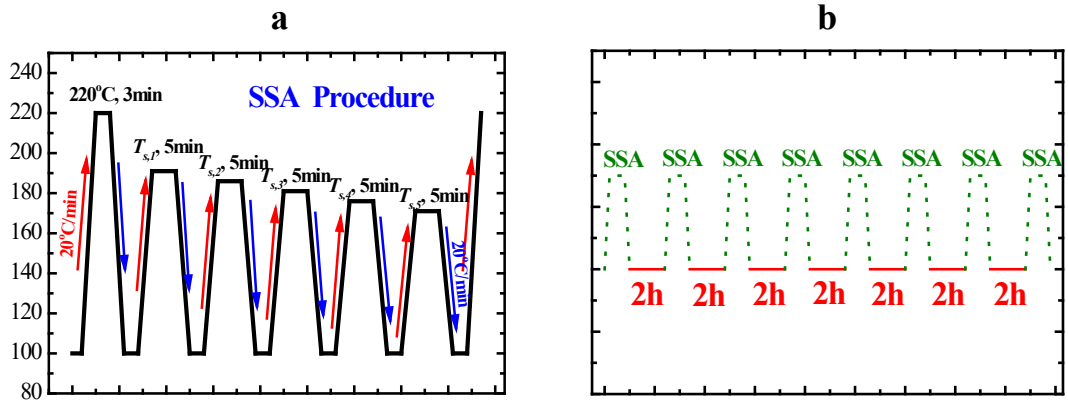

Figure 1. Experimental diagram: (a) Schematic representation of the SSA thermal protocol. (b) Combination of the SSA procedure and isothermal heat treatment for studying the lamellar thickness evolution and kinetics of PA1012.

Kinetic Studies of PA1012 chain structural evolution by SSA. The combination

of the SSA procedure and isothermal treatment for studying the lamellar thickness evolution (through the changes in thermal fractions melting) and kinetics for PA1012 was carried out in the DSC instrument. The N_2 atmosphere in DSC provided inert protection and removal of small molecular condensates. The procedure is described in Figure 1b. In the schematic diagram, the green line represents a complete SSA process, and the red line represents 2 h at the specific temperature. Each SSA revealed the fractionation of the sample after the cumulative isothermal treatment time. The total time of isothermal heat treatment was 14 h. The isothermal temperatures were set as 140, 170, 190, 210, 230, and 250 °C separately. The $T_{s,ideal}$ value after isothermal treatment changed less than 1 ºC after the isothermal thermal protocols applied, hence it was considered to be always kept constant.

Isothermal Crystallization. The samples were first subjected to different time periods at 250 °C, as in the above procedure for kinetic studies by SSA (i.e., the samples after isothermal treatment and SSA procedure). Then, isothermal crystallization experiments were carried out to measure the overall crystallization rates of the samples. The samples were melted for 5 min at 230 °C to erase thermal history and crystalline memory. Then, the samples were rapidly cooled to the chosen isothermal crystallization temperature (T_c) at an apparent cooling rate of 300 °C/min (the real cooling rate was 234 °C/min as indicated by the slope of a plot of measured temperature vs. time). We employed this fast cooling rate to try to avoid any further reactions after the heat treatment, even if some small errors are inevitably introduced when the isothermal

crystallization experiments were preformed, as some overshoot in temperature inevitably occurs when the experiment is switched from non-isothermal at 300 ºC/min nominal rate to the isothermal measuring mode. The appropriate T_c range for each sample was determined by preliminary tests to check that the samples did not crystallized during the cooling to the isothermal crystallization temperature.

Glass Transition Temperature Measurements. The samples were first subjected to different time periods at 250 °C, as in the above procedure for kinetic studies by SSA (i.e., the samples after isothermal treatment and SSA procedure). Then, the samples were melted for 5 min at 230 °C to erase thermal history and crystalline memory. Then, the samples were quenched to -150 °C by employing ballistic cooling and subsequently heated to 230 °C at 500 °C/min.

Rheological Measurements

Oscillatory shear experiments were performed with a Discovery Hybrid Rheometer (TA DHR-2) using parallel plates with diameters of 25 mm. Cyclic oscillation frequency sweep experiments without residual times between sweeps were performed with sweep rates ranging from 500 rad/s to 0.1 rad/s at 250 °C, with an amplitude of 1 % in the linear viscoelastic regime and with a continuous purge of nitrogen. Oscillation time sweep experiments were performed at 250 °C with a frequency of 1 Hz and amplitude of 3 % in the linear viscoelastic regime with a continuous nitrogen purge.

Thermo Gravimetric Analysis (TGA)

A PerkinElmer 8000 TGA was employed and calibrated before measurements. All

experiments were performed under high purity nitrogen. Sample weights of 3 mg were used. The program was set to heat from 50 °C to 550 °C at a rate of 10 °C/min.

Solubility Testing

The samples were first treated for different time periods at 250 °C. Then, the samples were dissolved in 1,1,1,3,3,3-hexafluoro-2-propanol (HFiP) at room temperature. Solvent HFiP was purchased from Aladdin Co., Ltd. (H107501). The concentrations of samples were 5 mg/ml.

RESULTS AND DISCUSSION

Effective Lamellar Thickness Fractionation

We explored a SSA protocol suitable for fractionating PA1012 before isothermal treatment. As indicated in the Supporting Information (Figure S1 and Figure S2), the SN results for PA1012 before isothermal treatment yielded a $T_{s,ideal}$ value of 191 ºC. As mentioned in the Experimental Section, Figure S3 shows 4 fractions obtained after a 5-step SSA protocol, for which the $T_{s,ideal}$ produced only self-nucleation without annealing. Each melting peak of the fractions corresponded to the melting of crystallites with different average lamellar thicknesses that were formed and annealed at each T_s. The relationship between lamellar thickness and melting point is explained by the Gibbs-Thomson equation[25-26]. SSA has been employed to quantitatively determine the distribution of lamellar thicknesses resulting from T_m values and the relative latent heats of fusion for each fraction[24, 27-30]. Figure S3 shows the expected linear relationship between the T_m and T_s temperatures, demonstrating that the SSA we designed was a superposition of several SN steps and indicating that it is reasonable.

We used the Gibbs-Thomson equation to generate a distribution of lamellar thicknesses (L_c) by employing the DSC traces obtained after SSA treatment:

$$L_c = \frac{2\sigma_e T_m^0}{\Delta H_m^0 (T_m^0 - T_m)} \quad (1)$$

where T_m^0 is the equilibrium melting point (479 K[31]), ΔH_m^0 is the bulk melting enthalpy per unit volume for a fully crystalline polymer and σ_e is the fold surface free

energy. No data exists in the literature on ΔH_m^0 and σ_e values for PA1012. For polyamides, a procedure to estimate the equilibrium melting enthalpy based on the additivity of properties can be used as an approximation. Xenopoulos et al.[32] normalized the contributions of given groups and determined values of 3.8 and 5.0 kJ/mol for the amide and methylene groups, respectively. Therefore, we used these values to calculate the approximate equilibrium melting enthalpy for PA1012 as 294 J/g and then converted this into the equilibrium bulk melting enthalpy by using the calculated density ρ_c of perfect crystals (α form) of PA1012[33]; $\Delta H_m^0 = 294 \times 1.134 = 333\ \mathrm{J/cm^3}$.

The Lauritzen and Hoffman (LH) theory[34] can be employed to fit spherulitic growth data. From the LH plots, the value of K_g^G allows the product of the lateral surface free energy σ and σ_e to be calculated from the following formula[35].

$$K_g^G = \frac{jb_0\sigma\sigma_e T_m^0}{k\Delta H_m^0} \quad (2)$$

where *j* is a parameter which depends on the operating crystallization regime and it is equal to 4 for regime I and III, and equal to 2 for regime II. The LH theory considers that the growth rate is a function of the competition between deposition rate of secondary nuclei (*i*) and lateral surface spreading rate (*g*). As a result, three different crystallization regimes are produced. When $i << g$ the sample is under regime I and it is usually found at very low degrees of supercooling. In the second regime, or regime II, *i* has values of the order of *g*. Regime II can be found at intermediate supercoolings. Finally, when $i > g$, the sample enters regime III and this only occurs at very high

degrees of supercooling. Regime behavior varies from polymer to polymer.

Therefore, we should first obtain the K_g^G value for PA1012 to estimate the product of σ and σ_e. The LH theory can be used to fit growth rate data, which yields the energy barriers associated to the secondary nucleation process, according to the following equation:

$$G = G_0 exp\left[\frac{-U^*}{R(T_c-T_0)}\right]\left[\frac{-K_g^G}{T_c\Delta T f}\right] \quad (3)$$

where G_0 is a growth rate constant, U^* is the activation energy related to molecular diffusion to the growth front (a value of 1500 cal/mol is frequently used), and R is the gas constant. T_c is the crystallization temperature, T_0 is the temperature at which chain movements freeze (calculated as $T_0 = T_g - 30\ ^oC$) and ΔT is the supercooling defined as $(T_m^0 - T_c)$. The factor f is a temperature correction term given by: $\frac{2T_c}{T_m^0+T_c}$.

Plotting $lnG + \frac{U^*}{R(T_c-T_0)}$ versus $\frac{1}{T_c\Delta T f}$ should yield a straight line and its slope should be equal to $-K_g^G$. Having the value of K_g^G, the product of σ and σ_e can be calculated.

However, there are no reports about the K_g^G value for PA1012 because it is difficult to get it, as nucleation density in PA1012 is high and spherulites are small and quickly grow to impinge with one another. However, the LH theory can also be applied to fit the overall isothermal crystallization data by DSC. By using the value of the inverse of the half-crystallization time ($1/\tau_{50\%}$) determined by DSC instead of G as the characteristic rate, Equation (3) has to be modified as follows[36-37]:

$$1/\tau_{50\%} = 1/\tau_{50\%,0}\ exp\left[\frac{-U^*}{R(T_c-T_0)}\right]\left[\frac{-K_g^\tau}{T_c\Delta Tf}\right] \quad (4)$$

where all the terms have been defined in Eq. (3), except for K_g^τ. K_g^τ is different from K_g^G. K_g^τ represents a parameter proportional to the energy barrier for both primary nucleation and growth (because it is derived from DSC data that takes into account both nucleation and growth) and K_g^G represents a parameter proportional to the energy barrier for secondary nucleation or only growth (obtained from polarized optical microscopy growth only data). Besides, the K_g^τ is actually better for applying the Gibbs-Thomson equation to DSC data, as it also comes out of fitting DSC data.

Figure 2a shows that the experimentally determined $1/\tau_{50\%}$ as a function of T_c. Figure 2b shows that the way of fitting the experimental data of isothermal crystallization in DSC (Figure 2a) to the LH theory by plotting $ln(\tau_{50\%}) + \frac{U^*}{R(T_c-T_0)}$ versus $\frac{1}{T_c\Delta Tf}$, a straight line is given and K_g^τ can be determined from the slope of the plot.

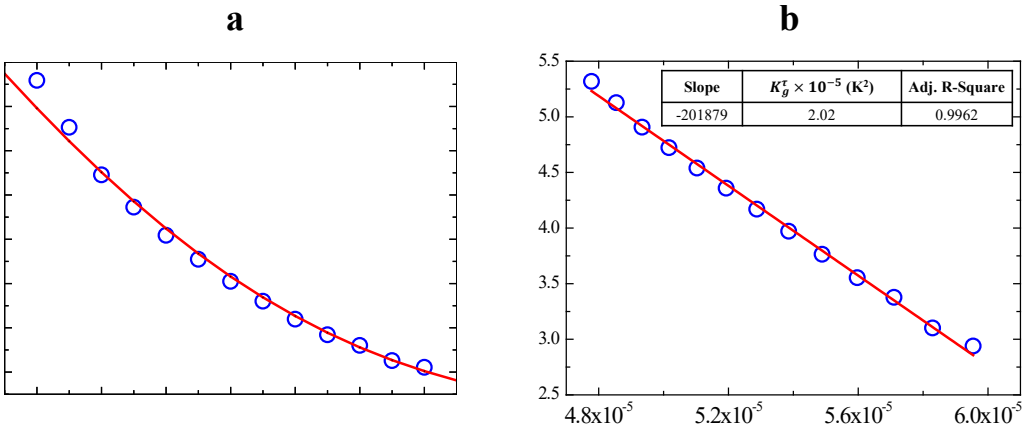

Figure 2. (a) $1/\tau_{50\%}$ as a function of isothermal crystallization temperature for PA1012. (b) Lauritzen and Hoffman (LH) plot. The continuous lines show the LH fit on top of the experimental data.

From Figure 2b, K_g^τ was determined to be 2.02x10^5 K^2. Based on the following references[6, 38-40] for different polyamides, a Lauritzen Z-test[41] was applied to investigate the crystallization regime in the selected temperature region. The results indicate that PA1012 is crystallizing in Regime I. Hence, j should be taken as equal to 4 in Eq. (2). The detailed introduction and procedure of Lauritzen Z-test for PA1012 is given in the Supporting Information (Table S1).

Next, we calculated an average of the product of $\sigma\sigma_e$ as 1310 erg^2/cm^4. The σ value was then determined from the following empirical formula[34]:

$$\sigma = \alpha \Delta H_m^0 (a_0 b_0)^{1/2} \quad (5)$$

where a_0 is the width of the chain in the crystal, b_0 is the thickness of a

monomolecular layer of the crystal, ΔH_m^0 is the melting enthalpy per unit volume of a 100% crystalline polymer, and α is an empirical constant that usually ranges between 0.1 and 0.3. Typically, α is estimated as 0.1 for polyolefins, 0.24 for polyesters, and 0.3 for the majority of other polymers[39]. Here, we chose α=0.3 for PA1012. Therefore, σ resulted equal to 4.03×10^{-2} J/m^2, and σ_e was determined to be 0.032 J/m^2.

Finally, we obtained the Gibbs-Thomson equation for PA1012. The experimental melting points determined in the DSC scan of Figure 3a (x axis) were transformed into the lamellar thickness values in Figure 3b by using the Gibbs-Thomson equation.

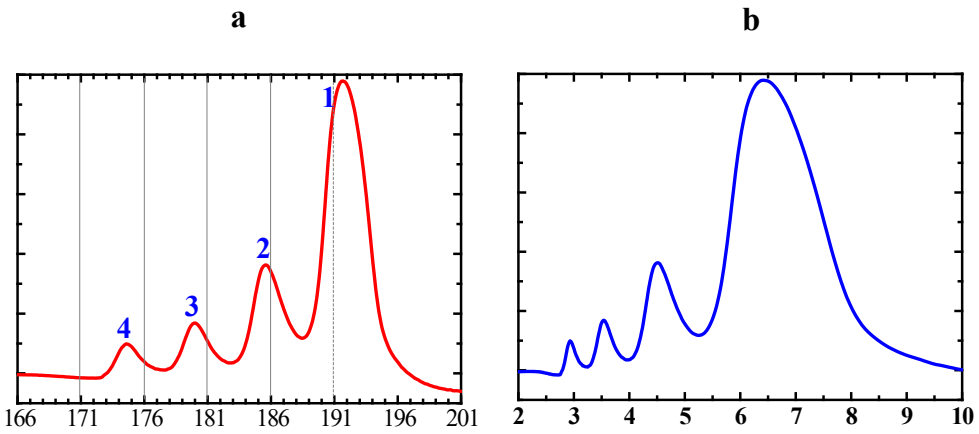

Figure 3. (a) SSA final heating runs and (b) lamellar thickness distribution calculated by employing the Gibbs-Thomson equation with the data presented in (a).

We estimated the average lamellar thickness (L_c) (this value was listed in the third column of Table 1) from the SAXS results described in Figure S4; these were determined by stepwise heating at 20 °C/min (this heating rate was identical to that in

the final heating step of the thermal fractionation) to 172 °C, 177 °C, 183 °C and 189 °C. The exposure time at each selected temperature was 10 s. The sample measured by SAXS was the DSC sample subjected to the SSA thermal protocol without the final melting step.

Table 1 summarizes the L_c values derived from the SAXS results and calculated by using Eq. (1), and the corresponding DSC melting peak values. To calculate an approximate average L_c value that could be compared to the L_c value obtained by SAXS, we use the mass fraction weighted average lamellar thickness value ($L_{c,avg}$) (this value was listed in the last column of Table 1) determined from the integrations of areas under the DSC endotherms.

Table 1. Average lamellar thicknesses values obtained by SAXS and by the Gibbs-Thomson equation using DSC data.

T_s (°C)	$T_{m,peak}$ [a] (°C)	L_c [b] (nm)	Gibbs-Thomson [c]	
			L_c (nm)	$L_{c,avg}$ [d] (nm)
171	191.7, 185.6, 180.0, 174.6	4.8	6.4, 4.5, 3.5, 2.9	5.6
176	191.7, 185.6, 180.0	4.8	6.4, 4.5, 3.5	5.7
181	191.7, 185.6	4.9	6.4, 4.5	6.0
186	191.7	5.0	6.4	6.4

[a] Multiple melting peaks were observed in the final heating curve after SSA. [b] Average L_c obtained from SAXS profiles using the one-dimensional electron density correlation function (EDCF). [c] L_c values obtained from the Gibbs-Thomson equation using the measured melting peak values. [d] Weighted L_c averages determined according to the integration ratio in DSC.

The SAXS results can be used to validate the values calculated by the Gibbs-Thomson equation. The $L_{c,avg}$ calculated by the Gibbs-Thomson equation was in good agreement with the L_c measured by SAXS. The average lamellar thickness values obtained by SAXS and DSC increased slightly upon heating, which means that the interlamellar distance gradually increased due to the fact that the thinner lamellar stacks melted first followed by the thicker ones.

SSA is not very sensitive to the molecular weight distributions of some polymers. However, the structural regularity of PA1012 is relatively high, and its molecular structure exhibits no branching. When there are no defects along the chains, the

macromolecular end groups will be excluded from the amorphous regions, and fractionation will occur due to differences in chain lengths. Therefore, the fractionation results for PA1012 could reflect the distribution of molecular chain lengths, those that can enter the crystal lattice. In the SSA results obtained during thermal treatment, the change in the horizontal axis qualitatively could correspond to the change in the molecular chain length, and the integration of each fraction could correspond to the number of molecules with that chain length. However, if crosslink reactions occur during thermal treatments at high temperatures, chain linearity will be interrupted facilitating fractionation.

We attempted to correlate the evolution of lamellar thickness and its distribution with changes in: molecular weight and its distribution and chain structure (e.g. changes due possible crosslinking reactions) by using a combination of the SSA procedure and isothermal treatments.

Evolution of Lamellar Thickness and Its Distribution under Different Temperature Fields

Figure 4a and Figure 4b show the final heating runs determined after cumulative isothermal treatment times at 170 °C and 250 °C. Figure S3(c) and Figure S3(d) show the expected linear relationships between the T_m and T_s temperatures, demonstrating that the SSA protocols we designed comprised a superposition of several SN steps, thereby indicating that the protocols were reasonable.

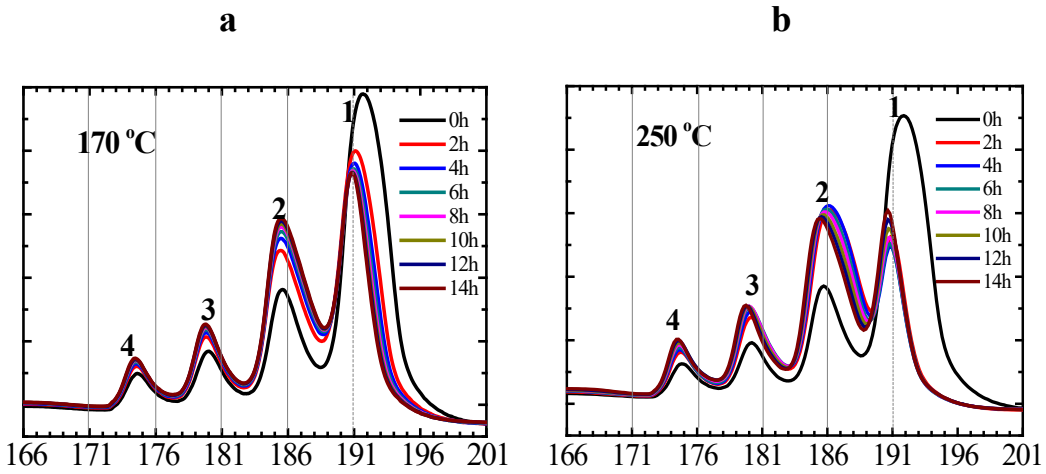

Figure 4. Final heating runs after cumulative isothermal heat treatment times at (a) 170 °C and (b) 250 °C. The thermal fractions are numbered from 1 to 4 on top of each melting peak.

We defined the highest temperature peak on the horizontal axis as the first fraction and the lowest temperature peak as the fourth fraction (see the numbers in Figure 4). Figure 4a and Figure 4b show that the melting peak of the first fraction was shifted to lower temperatures with increasing isothermal treatment time. These results were somewhat unexpected. The thermal treatment at high temperatures (170 and 250 ºC) should have increased the molecular weight, which would increase the lamellar thickness corresponding to the first fraction; the actual results varied in the opposite direction. For example, as mentioned in the Introduction section, at lower temperatures, SSP would occur and would increase the molecular weight. Therefore, we should first confirm whether degradation occurred.

Figure 5a indicates that no degradation occurred after cumulative isothermal

treatment at 250 °C for 14 h, since the TGA curve was shifted to the right. Figure 5b also proves that no degradation occurred. The oscillation time sweep experiment was performed in the linear viscoelastic regime, which is an effective method for investigating structural changes occurring within temperature fields[42-45]. With increasing isothermal time, the elasticity modulus increased, which suggested that a reaction enhancing viscosity must have occurred because the end groups of LCPAs were still reactive, as mentioned above. However, this viscosity-increasing reaction did not increase the lamellar thickness because other structural changes may have taken place during the isothermal treatment.

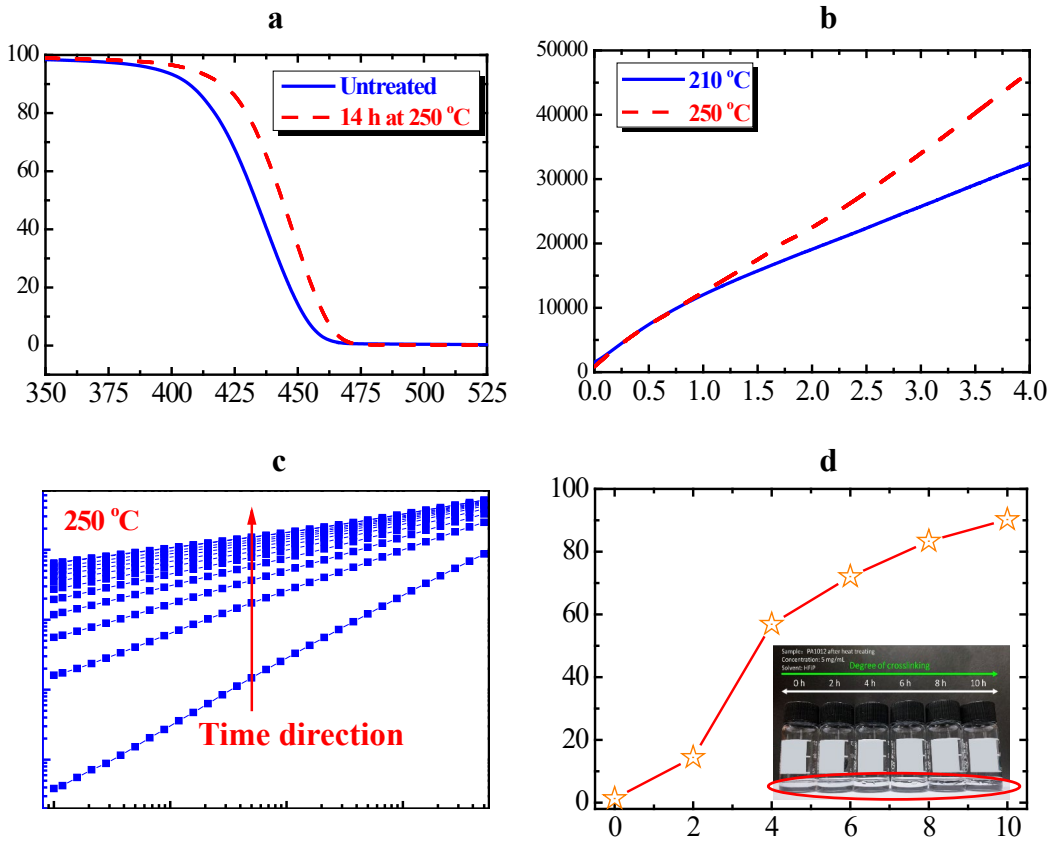

Figure 5. (a) TGA results obtained before and after isothermal treatment for 14 h at 250 °C. (b) Oscillation time sweeps at 210 °C and 250 °C. (c) Cyclic oscillation frequency sweep at 250 °C. (d) Degree of crosslinking and results of dissolution at room temperature after treatment at 250 °C for different isothermal time periods.

The results in Figure 5c revealed that the elasticity modulus deviated from the scaling law in the terminal region and developed a plateau at low frequencies. This result indicated that a crosslinked structure was formed during the high temperature isothermal treatment[46-49]. So, was this crosslinking process physical or chemical in nature? Was it reversible or irreversible? According to Figure 5d, a chemically crosslinked structure would not be soluble, and the proportion of this structure increased

with increasing time.

Figure 6a shows that the value of T_g was increased with increasing isothermal treatment time. This also proved that a chemically crosslinked structure formed hindering the long range motions of the polyamide chains, resulting in an increase in T_g.

Isothermal overall crystallization experiments were performed by DSC to determine the half-crystallization times of the samples. The relative crystallinity (α) could be obtained through the ratio of the crystallization peak area before time over its total area. The half-crystallization time ($\tau_{50\%}$) corresponds to the crystallization time for the relative crystallinity α=50 %. The inverse of the half-crystallization time could provide an experimental measure of the overall crystallization rate (i.e., the inverse of the half-crystallization time, $1/\tau_{50\%}$). This overall crystallization rate includes nucleation and growth. Figure 6b shows the overall crystallization rate for PA1012 as a function of T_c with different isothermal times at 250 °C. Some studies[50] have demonstrated that the overall crystallization rate first increased as the molecular weight increased, then reached a maximum, and finally decreased. For most commercial polymers, such as polyamides, molecular weights are high enough that they are in the molecular weight range in which the overall crystallization rate decreases with increasing molecular weight. The results presented in Figure 6b are consistent with increases in molecular weight (by chain extension or crosslinking) which cause a decrease in the overall crystallization rate.

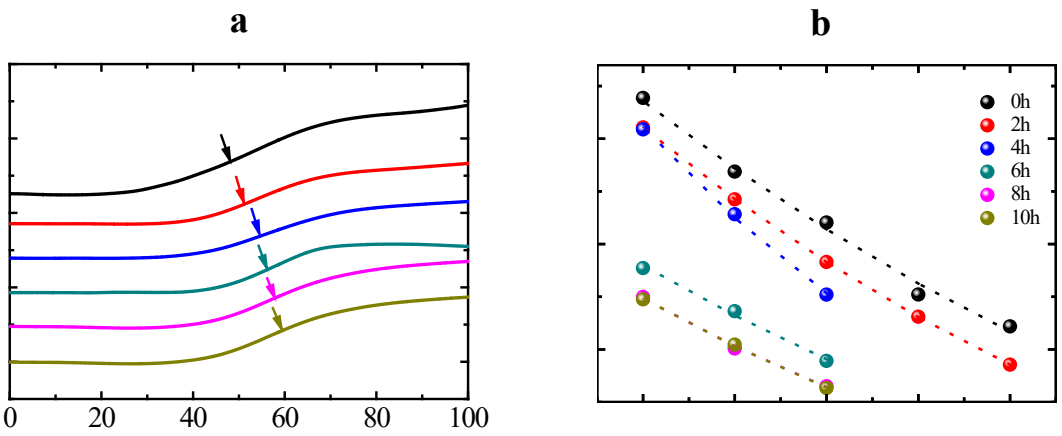

Figure 6. (a) DSC heating scans after quenching treatment at 250 °C for different isothermal time periods. (b) Overall crystallization rate ($1/\tau_{50\%}$) versus isothermal crystallization temperature for PA1012 treated at 250 °C for different isothermal time periods. The dotted lines show the LH fit on top of the experimental data.

Figure S6 also shows that with the extension of isothermal times spent at a fixed temperature, T_c and T_m decreased, a result consistent with a change from linear to a crosslinked structure. Any interruption in the linear crystallizable sequence causes a depression in melting temperature as it limits the achieved lamellar thickness.

According to the gel permeation chromatography (GPC) results in Table S2, the molecular weight decreased with increasing time spent at 170 °C. However, thermal treatment at 170 ºC should have increased the molecular weight. Considering that PA1012 was crosslinked during the heat treatment, the GPC test result was for the dissolved fraction, that is, the molecular weight of the crosslinked fraction could not be measured by GPC. Therefore, these results also indicated the occurrence of

crosslinking. The molecular weight decreased with increasing time spent at 170 °C and the molecular weight and distribution (MWD) decreased, which may also correspond to an increase in the degree of crosslinking.

Was it only the chemical structure that caused the viscosity in Figure 5b to increase over time? We think that in addition to the formation of a chemical network, there should have also been linear chain growth competing reactions. We also speculate that following the evolution of the SSA fractionation profiles, i.e., not only the peak melting points but also the areas under each fraction, we may be able to measure these two competing reactions: chain growth versus crosslinking reactions.

Kinetics of Lamellar Thickness and Its Distribution Evolution at Different Temperatures

The isothermal temperatures employ to treat the samples at high temperatures were separately set as: 140, 170, 190, 210, 230 and 250 °C in Figure S7.

Due to more obvious changes in the integrated area than in the melting points of the fractions, we chose to compare the former values resulting after different isothermal treatments at the selected temperatures. The integrated area of the first or second fraction was plotted against the total integrated area as a function of the treatment time, as shown in Figure 7. The specific integration method is shown in the Supporting Information (Figure S5).

Figure 7 (a-b) shows that at lower isothermal temperatures (140 °C, 170 °C and 190 °C) and with increasing time, S_1/S decreased and S_2/S increased, while the lamellar

thickness and its distribution (i.e., the melting point distribution of each thermal fraction) narrowed. We could see that the trend for changes in the integrated area (change in the slope of the curve) became larger, which meant that the reaction rate increased as the temperature increased.

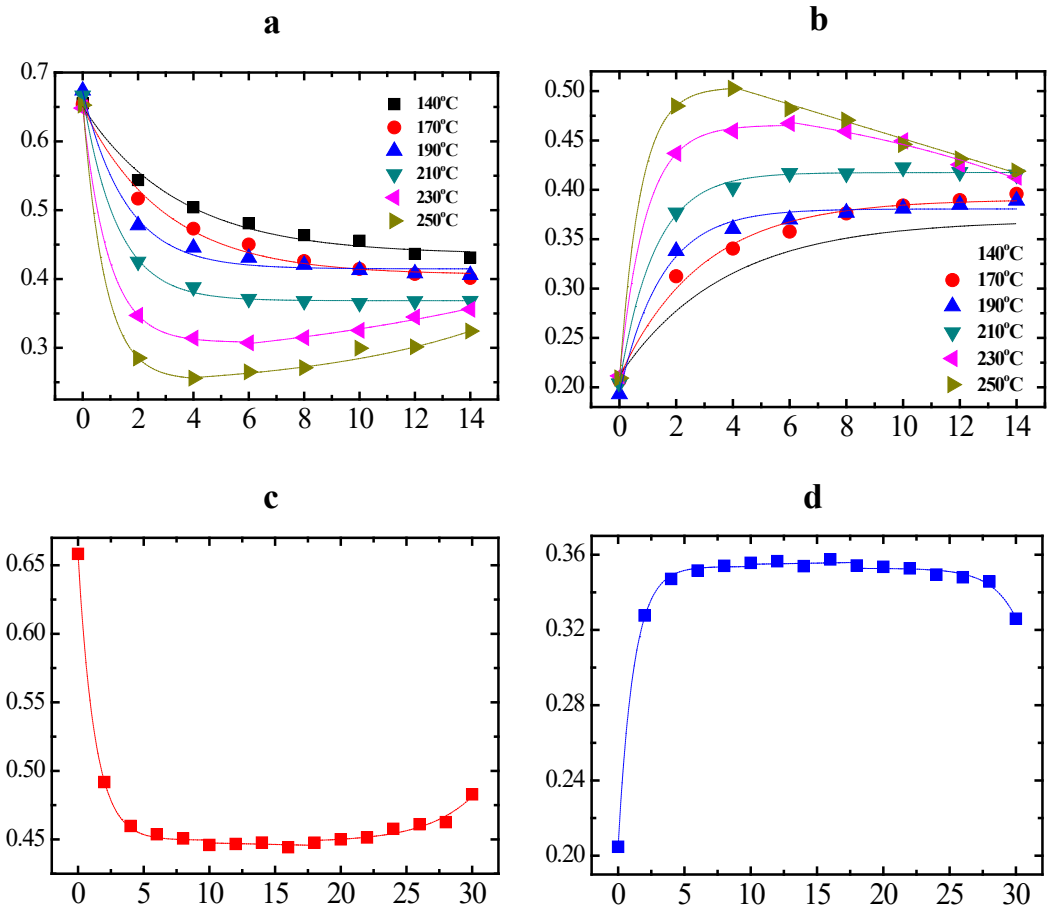

Figure 7. Integrated area of (a) the first (S_1/S) or (b) second (S_2/S) thermal fraction against the total integrated area as a function of isothermal time at 140, 170, 190, 210, 230 and 250 °C and as a function of times up to 30 h at 190 °C (c-d). The dashed lines show the fit on top of the experimental data.

However, at higher isothermal temperatures (210 °C, 230 °C and 250 °C), the

lamellar thickness and its distribution first turned narrower, which was the same behavior seen at lower isothermal temperatures, and then turned wider, which was different from the behavior seen at lower isothermal temperatures. Hence, a minimum in the value of the area of the first fraction appears for the data corresponding to 230 and 250 ºC in Figure 7a and a corresponding maximum in Figure 7b for the second thermal fraction. Figure 4 clearly shows that while the size (area) of the first thermal fraction decreases with the thermal treatment time, the second thermal fraction area correspondingly increases.

As the isothermal temperature was increased to 230 °C and 250 °C, maximum/minimum values (i.e., for the first/second thermal fractions) in the data remained. The higher the isothermal temperature was, the shorter the time corresponding to the appearance of maximum/minimum values. We decided to explore if there was a "time-temperature equivalence" that could describe a general trend.

Therefore, we prolonged the isothermal treatment time to 30 h at 190 °C, as indicated in Figure 7(c-d). Figure 7c shows that after 15 h at 190 °C, a minimum appears in the plot of the normalized area of the first thermal fraction, indicating a recovery behavior. At shorter times the crosslinking reaction dominates and makes the area of the first thermal fraction smaller, but at longer times at 190 ºC (longer than 15h) it would seem that chain extension reactions are now more important leading to a recovery of the area of the first thermal fraction.

A mirror image of Figure 7c is represented in Figure 7d. The reason for this

behavior is that the second thermal fraction grows at the expense of the decrease in the first fraction. For every long linear chain interrupted by a crosslinking point, two shorter ones are generated, hence the increase in the second (and third and fourth) thermal fraction areas that can be seen in Figure 4. Therefore, for the second fraction, a maximum in area is found when the contributions of crosslinking and chain extension is balanced. The fact that the maximum/minimum could be reached either by increasing the temperature or by prolonging the time confirmed a "time-temperature equivalence".

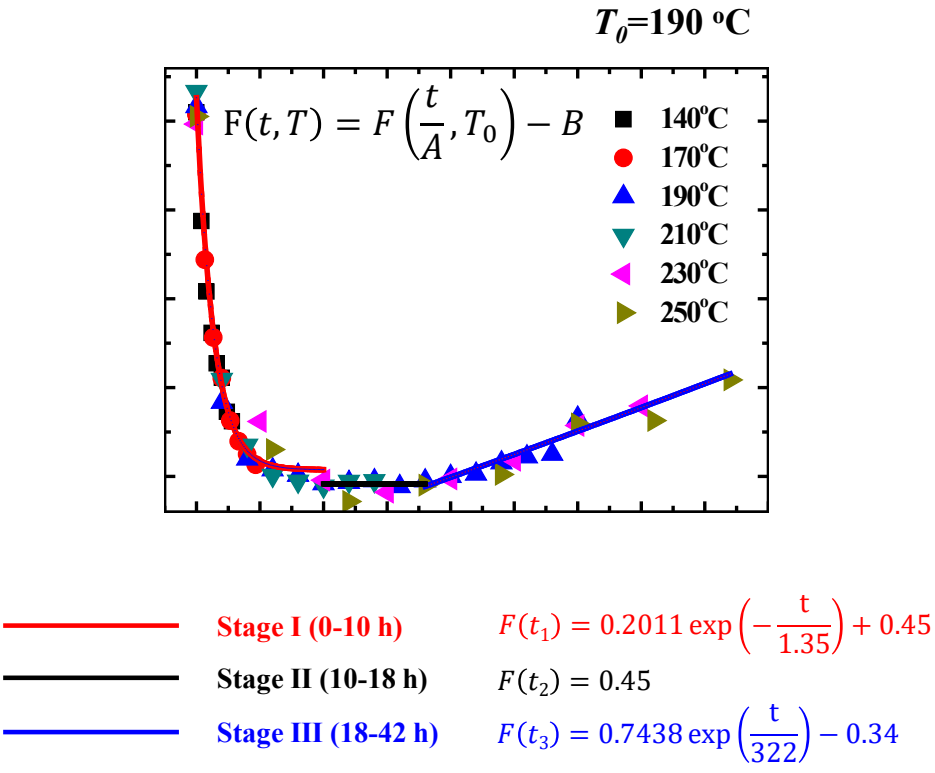

Figure 8. Fit of the "time-temperature equivalence" main curve. The reference temperature (T_0) was 190 °C.

The curves at different temperatures were shifted and superposed to build a master

curve along the time axis for a reference temperature (T_0) of 190 °C, as shown in Figure 8. The superposition formula is given by Eq. (6):

$$\mathrm{F}(t,T) = F\left(\frac{t}{A}, T_0\right) - B \quad (6)$$

where A and B are the t-shift factor and the f-shift factor, respectively, relative to different temperatures. T_0 is the reference temperature (190 °C here), and T is the isothermal treatment temperature. The relationships between A and B and temperature are shown in Table S3 and Figure S8.

We also fit the main curve and divided it into three different stages, as shown in Figure 8. In this way, we could consider the mechanisms separately.

Mechanism for the Lamellar Thickness Evolution of PA1012 Induced by Linear Chain Growth and Chemical Crosslinking

Two structural changes, linear chain growth (i.e., chain extension) and chemical crosslinking, occurred during the isothermal treatments applied to PA1012 in the temperature range between 140 and 250 ºC.

The mechanism for the evolution of the lamellar thickness of PA1012 in the main curve at a reference temperature (T_0) of 190 °C is discussed below and is shown in Scheme 1.

Due to the unstable nature of the amide groups of PA1012, there will always be some active sites (secondary amines) that serve as potential sites for crosslinking, which could react with the end groups of the macromolecules (amine and carboxylic end groups) in polyamide materials. During thermal treatment, the molecular chains of

polyamides were broken to generate new active sites and molecular end groups.

1. Stage I (0-10 h at T_0)

At the beginning of the thermal treatment, there are relatively few end groups. Chemical crosslinking was easily accomplished with end groups that rapidly reacted with active sites. The crosslinking points occurred at the N atoms of PA1012, which was confirmed by the CPMAS ^{15}N NMR spectra shown in Figure S9 and Table S4.

CPMAS ^{15}N NMR measures the signal by stimulating H atoms linked to N atoms. As the number of H atoms linked to N atoms is larger, the signal would be stronger under the same scanning time and the same sample mass. The integrated area of the signal at 250 ºC for 14 h decreased, which meant the number of H atoms linked to N atoms decreased due to the crosslinking reaction occurring during the heat treatment, as shown in Scheme S1. This observation is similar with PA66[51].

There were two possible crosslinking structures that separately resulted from the reaction of an amine end group with a carboxylic acid end group in PA1012, as shown in Scheme S1. In this stage, the distribution of lamellar thicknesses became narrow and the lamellar thickness decreased, as indicated by the lowering of the melting peak and narrowing of the melting peak distribution. This increased the melt viscosity, as shown in Figure 5, and decreased the mobility of the chains and their ability to crystallize, as shown in Figure 6. At 170 °C and during the first four-hour isothermal time at 250 °C, the melting peak of the first thermal fraction shifted to the left, that of the second thermal fraction shifted to the right, while the area of the first thermal fraction decreased,

and the area of the second thermal fraction increased.

2. Stage II (10-18 h at T_0)

With increasing thermal treatment time, the number of end groups rapidly increased. The amidation reaction between carboxylic end groups and amine end groups resulted in linear chain growth. In this stage, linear chain growth and crosslinking occurred simultaneously, and the effect of the two competing reactions on the lamellar thickness is opposite. There was no change in lamellar thickness because the contributions of crosslinking and chain extension are balanced.

3. Stage III (18-42 h at T_0)

In this later stage, linear chain growing mainly occurred via reactions of chain end groups. The proportion of the first thermal fraction increased and that of the second fraction decreased with increasing thermal treatment time.

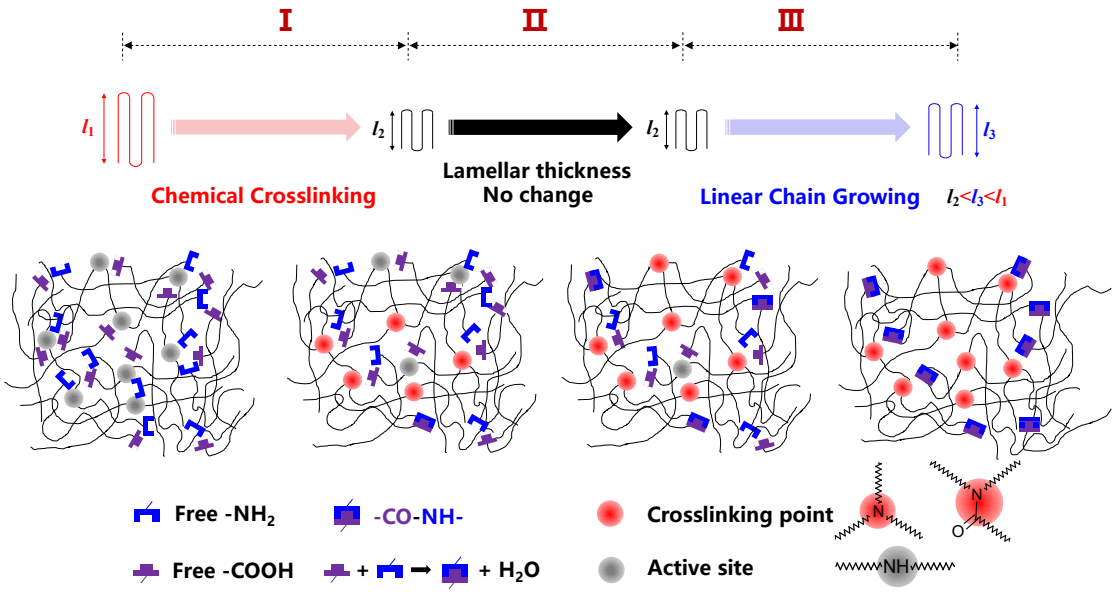

Scheme 1. Schematic of the mechanism for the evolution of lamellar thickness in PA1012 induced by linear chain growth and chemical crosslinking in the main curve at a reference temperature (T_0) of 190 °C.

Relationship between Structural Changes and Ultimate Properties

We also studied the effects of the structural changes caused by the applied thermal treatment on the performance of PA1012, especially on the mechanical properties.

Figure 9 and Table 2 show a comparison of the mechanical properties of PA1012 before and after isothermal heat treatment for 5 h at 250 °C. Both toughness and strength were obviously enhanced. The elastic modulus is almost the same value. That is because with increasing isothermal treatment time, the degree of crosslinking increased and the crystallization ability decreased in Figure 5, 6 and S6, and the nearly equal contributions of the two changes have the opposite effect to the elastic modulus.

In Figure 5a, the TGA curve was shifted to the right with increasing isothermal

time, which meant that the thermal stability and heat resistance were enhanced.

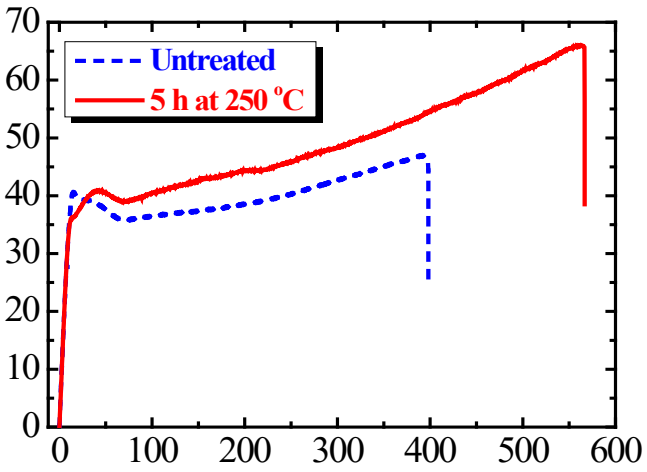

Figure 9. Stress-strain curve of PA1012 determined before and after isothermal treatment for 5 h at 250 °C.

Table 2. Comparison of the mechanical properties of PA1012 determined before and after isothermal treatment for 5 h at 250 °C.

Mechanical properties	Elastic modulus（MPa）	Yield strength（MPa）	Tensile strength (MPa)	Breaking elongation (%)	Impact strength (MJ/m^3)
Untreated	356±35	40±1	46±6	319±186	129±82
5 h at 250 °C	354±31	36±6	57±11	541±71	238±66

By controlling the temperature and time of thermal treatment, a preparation method for obtaining a PA1012 material with good toughness, high strength and high heat resistance was established. This method is very convenient and does not require other additives.

In the present work, we take PA1012 as our research object, which belongs to AABB type polyamides. AABB type polyamides are prepared by condensation of diamines and dicarboxylic acids. Due to the nature of condensation polymerization, the residual end groups of AABB type polyamides are still reactive. So, they should have the similar structural changes. Therefore, the research could also provide guidance for the structural evolution of all AABB type PAs during thermal treatment and suggested a design for high-performance materials.

CONCLUSIONS

In this study, the evolution of the melting points and their distribution (which are a reflection of lamellar thickness and its distribution) of PA1012 was investigated and was found to be affected by thermal protocols performed isothermally at high temperatures (140-250 ºC). SSA was used to fractionate PA1012 into 4 well defined thermal fractions corresponding to different melting points and therefore to different average lamellar thicknesses and their distributions. DSC, rheological measurements and solubility tests confirmed that both linear chain growth and chemical crosslinking occurred during the applied thermal treatments and exhibited opposing contributions to the lamellar thickness. Based on a “time-temperature equivalence” master curve at a reference temperature (T_0) of 190 °C, the mechanism for evolution of lamellar thickness was divided into three stages. In Stage I, chemical crosslinking easily occurred with active sites that reacted quickly with the end groups. In Stage II, linear chain growth

and crosslinking occurred simultaneously, while lamellar thickness and its distribution did not change. In Stage III, linear chain growth occurred primarily via reactions of chain end-groups. These structural changes that occurred during the applied thermal treatments enhanced the mechanical properties and heat resistance of the polymers. The thermal treatments applied to PA1012 provide a simple method and guidance for obtaining better toughness, higher strength and higher heat resistance in polyamide materials.

ASSOCIATED CONTENT

Supporting Information

Protocols of SN, SAXS, nonisothermal DSC, GPC, and Solid-State NMR tests, SN results, SSA results, SAXS and EDCF results, Lauritzen Z-test analysis and results, Integrated method for SSA results, nonisothermal DSC results, GPC results, temperature-dependent shift factors during building the master curve, Solid-State NMR results, and Scheme S1 showing the crosslinking structure occurred with thermal treatment.

AUTHOR INFORMATION

Corresponding Author

*E-mail xiadong@iccas.ac.cn and alejandrojesus.muller@ehu.es

ORCID

Lili Wang: 0000-0003-1974-4336

Xia Dong: 0000-0002-6409-7011

Alejandro J. Müller: 0000-0001-7009-7715

Dujin Wang: 0000-0002-2063-0873

Notes

The authors declare no competing financial interest.

ACKNOWLEDEMENTS

We acknowledge generous financial support from the following grants: National Key R&D Program of China (2017YFB0307600) and STS project of Chinese Academy of Sciences (KFJ-STS-QYZX-113). AJM acknowledges funding from the Basque Government through grant IT1309-19. We would like to thank the financial support provided by the BIODEST project; this project has received funding from the European Union's Horizon 2020 research and innovation programme under the Marie Sklodowska-Curie grant agreement no. 778092.

REFERENCES

1. Cai, Z.; Meng, X.; Ye, H.; Cong, C.; Wang, Y.; Cui, L.; Zhou, Q. Reinforcing polyamide 1212 nanocomposites with aligned carbon nanofibers. *Materials & Design.* **2014**, *63,* 691-698.
2. Wang, L.; Dong, X.; Gao, Y.; Huang, M.; Han, C. C.; Zhu, S.; Wang, D. Transamidation determination and mechanism of long chain-based aliphatic polyamide alloys with excellent interface miscibility. *Polymer.* **2015**, *59,* 16-25.
3. Zhu, P.; Dong, X.; Wang, D. Strain-Induced Crystallization of Segmented Copolymers: Deviation from the Classic Deformation Mechanism. *Macromolecules.* **2017**, *50,* 3911-3921.

4. Wang, L.; Dong, X.; Wang, X.; Zhu, G.; Li, H.; Wang, D. High performance long chain polyamide/calcium silicate whisker nanocomposites and the effective reinforcement mechanism. *Chinese Journal of Polymer Science.* **2016**, *34,* 991-1000.
5. Li, Y.; Zhu, X.; Tian, G.; Yan, D.; Zhou, E. Multiple melting endotherms in melt-crystallized nylon 10,12. *Polymer International.* **2001**, *50,* 677-682.
6. Ren, M.; Mo, Z.; Chen, Q.; Song, J.; Wang, S.; Zhang, H.; Zhao, Q. Crystallization kinetics and morphology of nylon 1212. *Polymer.* **2004**, *45,* 3511-3518.
7. Zhou, C.; Dong, S.; Zhu, P.; Liu, J.; Dong, X.; Wang, D. Effects of Linear Alicyclic Polyamide Chemical Structure on the Mechanical and Optical Properties. *Acta Polymerica Sinica (in Chinese).* **2021**, *52,* 297-303.
8. Zhou, C.; Qi, S.; Zhu, P.; Zhao, Y.; Xu, Y.; Dong, X.; Wang, D. The methylene infrared vibration and dielectric behavior monitored by amide group arrangement for long chain polyamides. *Polymer.* **2020**, *190,* 122231.
9. Yang, J.; Dong, W.; Luan, Y.; Liu, J.; Liu, S.; Guo, X.; Zhao, X.; Su, W. Crystallization and crosslinking of polyamide-1010 under elevated pressure. *Journal of Applied Polymer Science.* **2002**, *83,* 2522-2527.
10. Gao, Y.; Dong, X.; Wang, L.; Liu, G.; Liu, X.; Tuinea-Bobe, C.; Whiteside, B.; Coates, P.; Wang, D.; Han, C. C. Flow-induced crystallization of long chain aliphatic polyamides under a complex flow field: Inverted anisotropic structure and formation mechanism. *Polymer.* **2015**, *73,* 91-101.
11. Yoshioka, Y.; Tashiro, K. Structural change in the Brill transition of Nylon m/n (1) Nylon 10/10 and its model compounds. *Polymer.* **2003**, *44,* 7007-7019.
12. Yoshioka, Y.; Tashiro, K.; Ramesh, C. Structural change in the Brill transition of Nylon m/n (2) conformational disordering as viewed from the temperature-dependent infrared spectral measurements. *Polymer.* **2003**, *44,* 6407-6417.
13. Wang, L.; Dong, X.; Huang, M.; Wang, D. Transient microstructure in long alkane segment polyamide: Deformation mechanism and its temperature dependence. *Polymer.* **2016**, *97,* 217-225.
14. Flory; Paul, J. Polymerization process. US2172374 A, 1939.
15. Monroe, J.; George, C. Solid phase polymerization of polyamides. US72930558A, 1962.
16. Ikawa, T.; Shimamura, K.; Yokoyama, F.; Monobe, K.; Tanaka, Y. Solid State Polymerization of 12-Aminododecanoic Acid to Nylon 12 Under High Pressure. *Fiber.* **1986**, *42,* T403-T410.
17. Zhang, J.; Song, T.; Tian, G.; Liu, J. Preraration of Nylon 1212 with High VISCOSITYiscosity by the Solid State Post-Polymerization. *Engineering Plastics Application.* **2003**, *31,* 18-20.
18. Zhao, Q. X.; Yang, S. H.; Ying-Qiang, X. U.; Liu, M. Y.; Wang, Y. D.; Peng, F. U. Preparation of Nylon 1111 with High Viscosity by the Solid State Polycondensation. *Polymer Bulletin.* **2010**, *31,* 84-87.
19. Liu, X.; Wang, Y.; Liu, L.; Dong, X.; Wang, D. Time and Temperature Dependence of the Structural Evolution for Polyamide 1012. *Chinese Journal of Polymer Science.* **2020**, *38,* 993-998.
20. Müller, A. J.; Arnal, M. L. Thermal fractionation of polymers. *Progress in Polymer Science.* **2005**, *30,* 559-603.
21. Muller, A. J.; Hernandez, Z. H.; Arnal, M. L.; Sanchez, J. J. Successive self-nucleation/annealing (SSA): A novel technique to study molecular segregation during crystallization. *Polymer Bulletin.* **1997**, *39,* 465-472.
22. Liu, X.; Wang, Y.; Wang, Z.; Cavallo, D.; Müller, A. J.; Zhu, P.; Zhao, Y.; Dong, X.; Wang, D. The

origin of memory effects in the crystallization of polyamides: Role of hydrogen bonding. *Polymer.* **2020**, *188*, 122117.
23. Müller, A. J.; Michell, R. M.; Pérez, R. A.; Lorenzo, A. T. Successive Self-nucleation and Annealing (SSA): Correct design of thermal protocol and applications. *European Polymer Journal.* **2015**, *65,* 132-154.
24. Lorenzo, A. T.; Arnal, M. L.; Müller, A. J.; Boschetti de Fierro, A.; Abetz, V. High Speed SSA Thermal Fractionation and Limitations to the Determination of Lamellar Sizes and Their Distributions. *Macromolecular Chemistry and Physics.* **2006**, *207,* 39-49.
25. Lu, L.; Alamo, R. G.; Mandelkern, L. Lamellar Thickness Distribution in Linear Polyethylene and Ethylene Copolymers. *Macromolecules.* **1994**, *27,* 6571-6576.
26. Arnal, M. L.; Balsamo, V.; Ronca, G.; Sánchez, A.; Müller, A.; Caizales, E.; Navarro, C. Applications of Successive Self-Nucleation and Annealing (SSA) to Polymer Characterization. *Journal of Thermal Analysis and Calorimetry.* **2000**, *59,* 451-470.
27. Lorenzo, A. T.; Arnal, M. L.; Müller, A. J.; Boschetti de Fierro, A.; Abetz, V. Confinement effects on the crystallization and SSA thermal fractionation of the PE block within PE-b-PS diblock copolymers. *European Polymer Journal.* **2006**, *42,* 516-533.
28. He, F.; Zhang, L. Study on branching structure, melting, and crystallization of polyethylene prepared by nickel a-diimine catalyst covalently intercalated inside OapPOSS-modified laponite clay gallery. *Polymer Testing.* **2014**, *35,* 80-86.
29. Jokela, K.; Väänänen, A.; Torkkeli, M.; Starck, P.; Serimaa, R.; Löfgren, B.; Seppälä, J. Differential scanning calorimetry, small-angle x-ray scattering, and wide-angle x-ray scattering on homogeneous and heterogeneous ethylene-α-copolymers. *Journal of Polymer Science, Part B: Polymer Physics.* **2001**, *39,* 1860-1875.
30. Lorenzo, A. T.; Arnal, M. L.; Müller, A. J.; Lin, M.; Chen, H. SAXS/DSC Analysis of the Lamellar Thickness Distribution on a SSA Thermally Fractionated Model Polyethylene. *Macromolecular Chemistry and Physics.* **2011**, *212,* 2009-2016.
31. Li, Y.; Zhu, X.; Tian, G.; Yan, D.; Zhou, E. Multiple melting endotherms in melt-crystallized nylon 10,12. *Polymer International.* **2001**, *50*, 677-682.
32. Xenopoulos, A.; Wunderlich, B.; Subirana, J. A. Thermal properties of nylons related to polyglycine. *European Polymer Journal.* **1993**, *29,* 927-935.
33. Jones, N. A.; Atkins, E.; Hill, M. J.; Cooper, S. J.; Franco, L. Polyamides with a Choice of Structure and Crystal Surface Chemistry. Studies of Chain-Folded Lamellae of Nylons 8 10 and 10 12 and Comparison with the Other 2N 2(N + 1) Nylons 4 6 and 6 8. *Macromolecules.* **1997**, *30*, 3569-3578.
34. Hannay, N., *Treatise on solid state chemistry*. Plenum Press: 1976.
35. Patki, R.; Mezghani, K.; Phillips, P. J., Crystallization Kinetics of Polymers. In *Physical Properties of Polymers Handbook*, Springer: New York, 2007.
36. Lorenzo, A. T.; Müller, A. J. Estimation of the nucleation and crystal growth contributions to the overall crystallization energy barrier. *Journal of Polymer Science Part B: Polymer Physics.* **2008**, *46,* 1478-1487.
37. Safari, M.; Mugica, A.; Zubitur, M.; Martinez de Ilarduya, A.; Munoz-Guerra, S.; Muller, A. J. Controlling the Isothermal Crystallization of Isodimorphic PBS-ran-PCL Random Copolymers by Varying Composition and Supercooling. *Polymers (Basel).* **2020**, *12*, 17.

38. McFerran, N. L. A.; Armstrong, C. G.; McNally, T. Nonisothermal and isothermal crystallization kinetics of nylon-12. *Journal of Applied Polymer Science.* **2008**, *110,* 1043-1058.
39. Zhang, Q. X.; Mo, Z. S. MELTING CRYSTALLIZATION BEHAVIOR OF NYLON 66. *Chinese Journal of Polymer Science.* **2001**, *19,* 237-246.
40. Zhang, Q.; Zhang, Z.; Zhang, H.; Mo, Z. Isothermal and nonisothermal crystallization kinetics of nylon‐46. *Journal of Polymer Science Part B: Polymer Physics.* **1995**, *40,* 1784-1793.
41. Lauritzen, J. I. Effect of a finite substrate length upon polymer crystal lamellar growth rate. *Journal of Applied Physics.* **1973**, *44,* 4353-4359.
42. Esmizadeh, E.; Irani, A.; Naderi, G.; Ghoreishy, M. H. R.; Dobious, C. Effect of carbon nanotube on PA6/ECO composites: Morphology development, rheological, and thermal properties. *Journal of Applied Polymer Science.* **2018**, *135*, 45977.
43. Gupta, D.; Jassal, M.; Agrawal, A. K. Solution properties and electrospinning of poly(galacturonic acid) nanofibers. *Carbohydr Polym.* **2019**, *212,* 102-111.
44. Zhao, J.; Pan, H.; Yang, H.; Bian, J.; Zhang, H.; Gao, G.; Dong, L. Studies on Rheological, Thermal, and Mechanical Properties of Polylactide/Methyl Methacrylate-Butadiene-Styrene Copolymer/Poly(propylene carbonate) Polyurethane Ternary Blends. *Chinese Journal of Polymer Science.* **2019**, *37,* 1273-1282.
45. Wang, Y.; Wang, Z.; Zhu, P.; Liu, X.; Wang, L.; Dong, X.; Wang, D. Microphase separation/crosslinking competition-based ternary microstructure evolution of poly(ether-b-amide). *RSC Advances.* **2021**, *11,* 6934-6942.
46. Song, R.; Jiang, G.; Wang, K. Gelation mechanism and rheological properties of polyacrylamide crosslinking with polyethyleneimine and its plugging performance in air-foam displacement. *Journal of Applied Polymer Science.* **2018**, *135*, 45778.
47. Salehiyan, R.; Bandyopadhyay, J.; Ray, S. S. Mechanism of Thermal Degradation-Induced Gel Formation in Polyamide 6/Ethylene Vinyl Alcohol Blend Nanocomposites Studied by Time-Resolved Rheology and Hyphenated Thermogravimetric Analyzer Fourier Transform Infrared Spectroscopy Mass Spectroscopy: Synergistic Role of Nanoparticles and Maleic-anhydride-Grafted Polypropylene. *ACS Omega.* **2019**, *4,* 9569-9582.
48. Zhang, L.; Shi, W.; Wang, J.; Jin, L.; Hu, G.; Zheng, Q.; Xie, H.; Chen, P. Unique gelation and rheological properties of the cellulose/CO2-based reversible ionic liquid/DMSO solutions. *Carbohydr Polym.* **2019**, *222*, 115024.
49. Han, H.; Song, Y.; Zheng, Q. Rheological and Interfacial Properties of Colloidal Electrolytes. *Chinese Journal of Polymer Science.* **2019**, *37,* 1039-1044.
50. Giacobazzi, G.; Rizzuto, M.; Zubitur, M.; Mugica, A.; Caretti, D.; Müller, A. J. Crystallization kinetics as a sensitive tool to detect degradation in poly(lactide)/poly(ε-caprolactone)/ PCL-co-PC copolymers blends. *Polymer Degradation and Stability.* **2019**, *168*, 108939.
51. Schaffer, M.; Marchildon, E. K.; Mcauley, K. B.; Cunningham, M. F. Thermal Nonoxidative Degradation of Nylon 6,6. *Journal of Macromolecular Science: Reviews in Macromolecular Chemistry & Physics.* **2000**, *40,* 233-233.

Competition between Chain Extension and Crosslinking in Polyamide 1012 during High Temperature Thermal Treatments as Revealed by SSA Fractionation

Xuan Li,[1,2] *Lili Wang,*[1,3] *Dujin Wang,*[1,2] *Alejandro J. Müller,*[4,5,*] *and Xia Dong*[1,2,*]

For Table of Contents use only